

PAPER

Programmable and scalable assembly of a flexible hexagonal DNA origami


To cite this article: Congzhou Chen *et al* 2022 *Nanotechnology* **33** 105606

View the [article online](#) for updates and enhancements.

You may also like

- [Enhanced structural stability of DNA origami nanostructures by graphene encapsulation](#)
Aleksandar Matkovi, Borislav Vasi, Jelena Peši et al.
- [Towards atom manufacturing with framework nucleic acids](#)
Xiaoliang Chen, Bingjie Yan and Guangbao Yao
- [The potential of DNA origami to build multifunctional materials](#)
Kosti Tapio and Ilko Bald

Programmable and scalable assembly of a flexible hexagonal DNA origami

Congzhou Chen^{1,5} , Tingting Lin^{2,5}, Mingyuan Ma¹, Xiaolong Shi^{3,*} and Xin Li^{4,*}

¹Key Laboratory of High Confidence Software Technologies, School of Computer Science, Peking University, Beijing 100871, People's Republic of China

²Institute of Artificial Intelligence and Automation, Huazhong University of Science and Technology, Wuhan 430074, People's Republic of China

³Institute of Computing Science & Technology, Guangzhou University, Guangzhou 510006, People's Republic of China

⁴Department of Gynecology 2, Renmin Hospital of Wuhan University, Wuhan 430060, People's Republic of China

E-mail: xlshi@gzhu.edu.cn and lixinwhu@189.cn

Received 10 June 2021, revised 8 September 2021

Accepted for publication 15 September 2021

Published 15 December 2021



Abstract

Nanoscale structures demonstrate considerable potential utility in the construction of nanorobots, nanomachines, and many other devices. In this study, a hexagonal DNA origami ring was assembled and visualized via atomic force microscopy. The DNA origami shape could be programmed into either a hexagonal or linear shape with an open or folded pattern. The flexible origami was robust and switchable for dynamic pattern recognition. Its edges were folded by six bundles of DNA helices, which could be opened or folded in a honeycomb shape. Additionally, the edges were programmed into a concave-convex pattern, which enabled linkage between the origami and dipolymers. Furthermore, biotin-streptavidin labels were embedded at each edge for nanoscale calibration. The atomic force microscopy results demonstrated the stability and high-yield of the flexible DNA origami ring. The polymorphous nanostructure is useful for dynamic nano-construction and calibration of structural probes or sensors.

Supplementary material for this article is available [online](#)

Keywords: DNA origami, polymorphous nanostructure, changing patterns

(Some figures may appear in colour only in the online journal)

1. Introduction

DNA is considered an excellent material for nanofabrication. Seeman [1] initially proposed that DNA molecules could be programmable and biocompatible [2–5], flexible, rigid, and stable (single-strand pairs to double helix), and could exhibit a nanoscale size. DNA nanostructures have been used in numerous applications, including those pertaining to the construction of nanostructures, computing, nanocircuits, biosensors, and molecular robots [6–13]. Structural probes and sensors have shown marked potential applicability in the early diagnosis of

cancer and are deemed highly sensitive for detecting and targeting of viruses, such as dengue fever virus.

In 2006, Rothemund proposed DNA origami technology aimed at designing several two-dimensional nanostructures [14]. DNA origami involves a long circular (scaffold) strand that is tightly folded by numerous short (staple) strands in specific locations to a predesigned shape. Since its first report, various DNA origami structures have been developed [6, 15–20]. Researchers have demonstrated that arbitrary two-dimensional origami structures or wireframes can be constructed; furthermore, with additional advances, several three-dimensional structures have been developed [19–21]. Among such structures, flexible structures have attracted significant research interest.

⁵ CZC and TTL contributed equally to this work.

* Authors to whom any correspondence should be addressed.

The flexible origami motif plays a vital role in the assembly of molecular machines, including DNA motors, molecular tweezers, and nanoengines [22–24]. Wickham *et al* implemented a DNA-based molecular motor that could be used to navigate a network and to load or unload nanoparticles [25]. Additionally, Ketterer *et al* reported a DNA-based cylinder engine driven by a magnetic field [26].

Recently, DNA origami as an epitope for ligand-protein templates has gained prominence as an advancing frontier in disease research [27–32]. Settled origami epitopes have been constructed to explore the spatial tolerance of antibodies. Rinker *et al* showed that the distance could affect protein affinity on origami surfaces [27], and Shaw *et al* designed an origami receptor with distance-defined ligands to activate human breast cancer cells [28]. Moreover, Shaw *et al* further demonstrated that the binding distance of antigens was dominant in initiating antibody effector functions [29]. Finally, Veneziano *et al* constructed an icosahedron origami structure with a controlled antigen to mimic the human immunodeficiency virus immunogen, which demonstrated that antigen patterns could affect B-cell responses [30].

Settled origami structures cannot be used to coordinate the ‘induce-fit’ model of antibody-antigen interactions. To overcome this limitation, flexible origami structures have been proposed to match transient conformations. For example, Kwon *et al* designed a pentagram origami with the ability of multi-valent spatial pattern recognition for viral sensing and inhibition [31], and Zhang *et al* depicted transient antibody conformations using origami epitopes [32]. Hence, flexible origami structures with specific antigen patterns are useful as structural probes and sensors.

Flexible hexagonal origami was developed in the present study that could demonstrate the opening or closure of its edges and its shape was designed and programmed from a hexagonal ring to a pillar. Additionally, biotin-streptavidin labels were embedded at each edge of the hexagonal ring for easier detection, demonstrating the potential of this hexagonal structure to be used as a flexible biosensor or drug carrier.

2. Methods

2.1. Structure design

The caDNAno software (<http://cadnano.org>) with a honeycomb lattice module was used to design the hexagonal origami. Six double helices were bound together to enable the formation of an edge, and thirty-six helices of six edges formed the hexagonal origami structure. The design scheme is illustrated in figure 1. The spiral angle of these staple strands was 120°, conforming to the corner angle of each skeleton. Six skeletons were bound to each honeycomb edge, and these edges were connected end-to-end to enable the formation of hexagonal structures. Additionally, 8-nucleotide-long unpaired bases were retained at the end of each edge to prevent base stacking. The specific design details are illustrated in supplemental figure 1 (available online at stacks.iop.org/NANO/33/105606/mmedia).

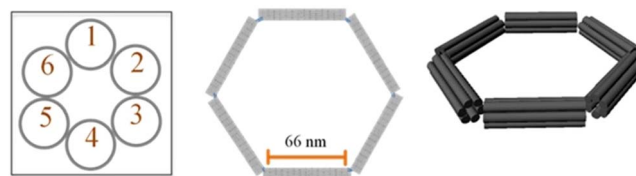


Figure 1. Design scheme of the hexagonal origami. Each edge was assembled by six double-helices and connected end-to-end. Three-dimensional view of the hexagonal origami.

2.2. Materials

All DNA strands were purchased from Sangon Biotech (Shanghai, China) and purified via high-performance liquid chromatography. The strands were dissolved in (1×) TEA buffer containing 12.5 mM Mg^{2+} to a final concentration of 100 μ M.

The origami was purified via electrophoresis using 1% agarose gel prepared with agarose dissolved in (1×) TAE buffer with 4SGelRed nucleic acid dye (BBI Life Science Corporation, Shanghai, China). Results of gel electrophoresis were shown in supplementary figure 3. The gel was immersed in (1×) TAE buffer and subjected to an 80 V, 100 mA direct current for 2 h. The target gel band was cut and incubated in (1×) TAE buffer at 25 °C for 12 h to separate the origami samples. Finally, the sample solution was enriched using an ultrafilter 100k tube (Millipore, Billerica, MA, USA).

The purified samples were scanned using the Multimode 8 serial atomic force microscope (AFM; Bruker Corporation, Billerica, MA, USA). Briefly, 10 μ l of a fresh sample was pipetted onto a clear mica surface and allowed to remain undisturbed for 5 min to enable complete adherence of the origami to the mica surface. Next, a mica structure with a steel disc was placed on the piezoelectric stage. When the AFM was set at the autoscan module, the piezoelectric stage approached the scanning probe (Fluid tip, Bruker Corporation). The autoscan model parameters were as follows: approaching force, 0.075 V; scan rate, 2 Hz; and lines, 1024.

3. Results and discussion

All staple and scaffold strands were mixed (1:10 ratio) at final concentrations of 5 and 50 nM for the M13 scaffold and staple strands, respectively. The mixed solution was annealed at temperatures ranging from 95 °C to 4 °C in a thermocycler (Hangzhou LongGene Scientific Instruments, Hangzhou, China). Next, the samples were purified by electrophoresis and condensed to a concentration of 2 nM in 50 μ l. Representative AFM images of the flexible hexagonal origami, which achieved a high yield, as shown in figure 2. The cyclic linked structures were randomly shaped, and the hinge angle of the edges was affected by the force between them. The length and width of a standard hexagon were 63.5 and 3.6 nm, respectively. The measured length was almost the same as that mentioned in the design scheme.

Biotin-streptavidin labels were added to the origami surface to extend five thymine nucleotides at the 3'-end of the outer staple strands (figure 3(a)). We selected six staple

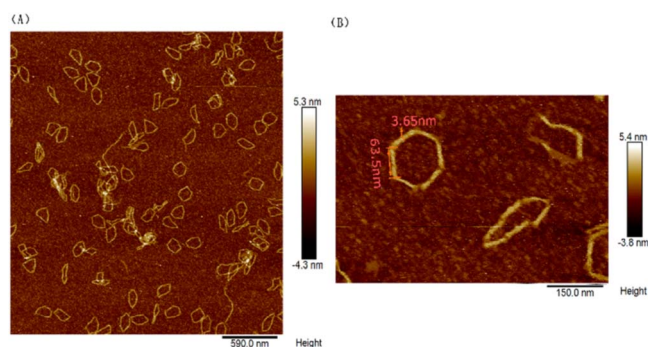


Figure 2. Atomic force microscopy imaging of hexagonal origami structures. (a) Origami structures scattered on the scanning surface. Scan size: $3\ \mu\text{m}$. (b) Detailed image of a hexagonal origami. The length and width are shown. Scan size: $750\ \text{nm}$.

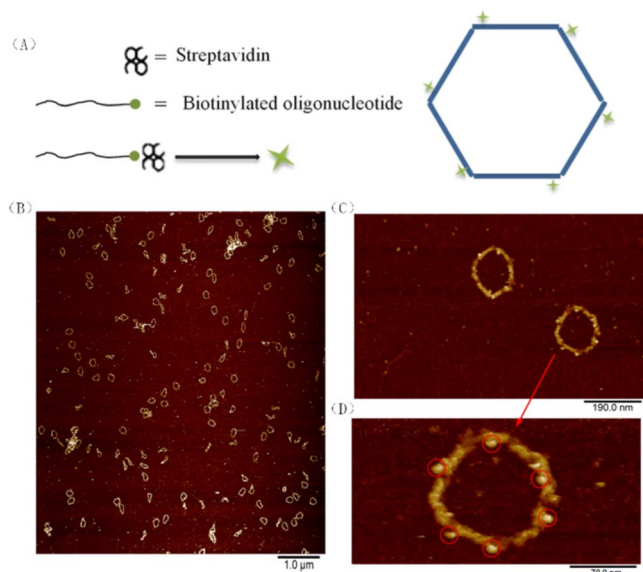


Figure 3. Biotin-streptavidin-labeled hexagonal origami structures. (a) Design scheme of the biotin-streptavidin embedded positions on the hexagonal origami. (b) Biotin-streptavidin-labeled origami structures, field of view: $10\ \mu\text{m}$. (c), (d) Detailed imaging of the origami structures. (c) Scale size: $1\ \mu\text{m}$. (d) Red circles indicate biotin-streptavidin molecules; scale size: $0.3\ \mu\text{m}$.

strands at each edge for biotin modification. The specific sequences and locations of these staple strands are illustrated in supplemental figure 2 and table 1.

First, the scaffold and staple strands were mixed and annealed to enable the formation of the origami structure, as described in the ‘Methods’ section. Next, the origami and biotinylated strands (Sangon Biotech Corp.) were mixed (1:20 ratio) and reannealed at temperatures ranging from $45\ ^\circ\text{C}$ to $4\ ^\circ\text{C}$ for 3 h. Finally, streptavidin solutions ($20\times$) were added to the samples and the mixture was incubated at $25\ ^\circ\text{C}$ for 1 h. All excess strands were purified using an ultrafilter tube in the final step. A representative AFM image of the biotin-streptavidin-labeled origami structures is presented in figure 3. The position of the biotin-streptavidin molecules did not precisely match the predicted design (figure 3(a)), possibly because of the drift of the molecules. When the scanning tip scrapes the dots, it may drag them,

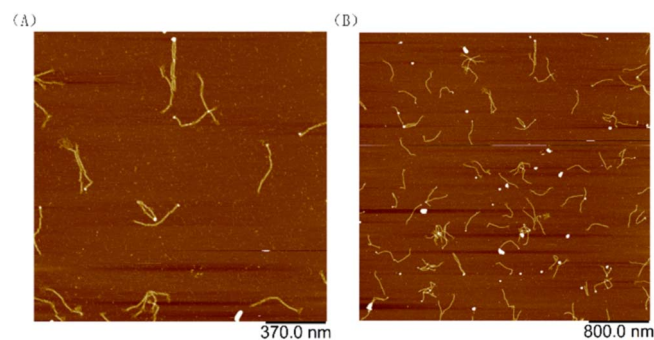


Figure 4. Linear origami with first five edges. (a) Field of view: $1.85\ \mu\text{m}$. (b) Field of view: $4\ \mu\text{m}$.

thereby altering their localization. Thus, hexagonal origami structures were successfully developed, and biotin-streptavidin molecules were effectively added to their surface.

We used six specific strands with biotin modification. The linking efficiency of biotin-streptavidin was predicted to be 100%; however, this value was nearly 70%. We obtained purification results, as shown in supplemental figures 1–13. Few biotin-streptavidin dots were blurry, and few dots might have been covered by the edges. However, the statistical results are reliable because of the greater number of purification results.

Additionally, we observed the presence of certain defective structures. Few structures did not link together to the hexagonal shape and others were randomly twisted. We scanned and statistically analyzed several purified samples. The ratio of defective structures was approximately 6%, as shown in supplemental figures 4–9 and in the Yield statistics section.

The hexagonal origami was cyclically assembled by six rod-like edges. According to the design schematic, loosening of the sixth edge will lead to formation of a short linear origami. The first five edges utilized 6030 nt of the M13 sequence, and the total length of the five edges should be 330 nm in a line. The length of the remaining M13 (1219 nt) can be 414.5 nm. In theory, the first five edges can be assembled in a line. Figure 4 shows the AFM results.

We obtained the short linear origami, as predicted. However, most structures were observed to be bent in solution, forming circular arcs rather than straight lines. Additionally, two-folded lines were found in this sample, as shown in the central region of figure 4(A). The top portion of the structure tended to form the joint end, as small white dots accrued at the top regions of these structures.

To compare the rigidity of the hexagonal origami structure and to obtain longer lines, we changed the design scheme and reprogrammed the origami into a linear structure (figures 5(a), (b)). Six edges were linked together through the bottom helix. The experimental protocol was the same as that used to develop the hexagonal origami. AFM imaging of the linear origami (figures 5(c), (d)) revealed that the origami shape was flexible because the 396 nm long double helix was not sufficiently rigid to maintain the six edges in a line.

The persistence length of the DNA double helix is 50 nm [33]; thus, the linear origami structures appeared as random

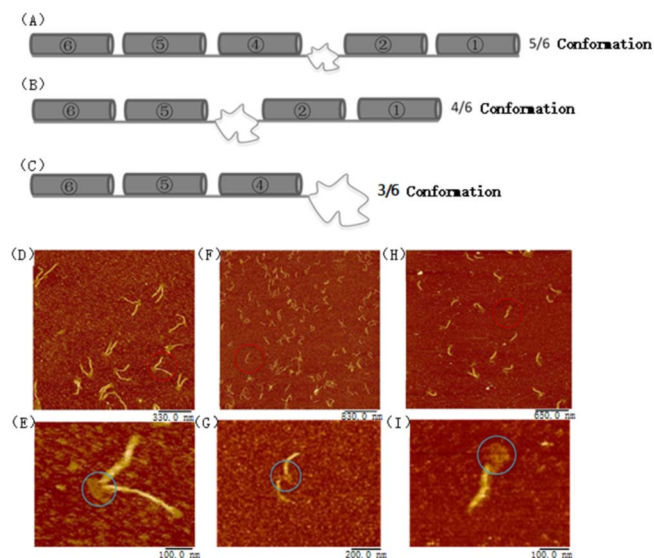


Figure 5. Different conformations of linear origami structures. Design scheme of (a) 5/6, (b) 4/6, and (c) 3/6 conformations. Atomic force microscopy images of (d), (e) 5/6, (f), (g) 4/6, and (h), (i) 3/6 conformations of the linear origami structures. Blue circles (e), (g), (i) indicate the opened edges that appear as ribbons and are connected to tubes (closed parts). Lines could be observed in the ribbon (e), whereas the opened parts in (g), (i) were not comparatively clear. Scan size: (d) 330, (e) 100, (f) 830, (g) 200, (h) 650, and (i) 100 nm.

strings in solution with six identifiable separate edges (figure 5(d)), with the bottom double helix functioning as a hinge that linked the edges.

The persistence length of B type DNA double helix is 50 nm. Therefore, the six-bundle DNA edge should be considered sufficiently robust. However, we found the linear origami was in a bent form in solution. We analyzed the persistence length of these linear origamis. The results are illustrated in supplemental figures 16 and 17. The average persistence length is 100 ± 18 nm (standard deviation is 18). The contour length and distance length of linear origamis were calculated via software and are shown in supplementary table 2, 'Lines with statistical analysis' section.

To construct the open-close pattern of the origami, a honeycomb edge was subjected to opening with some edges being closed and others being opened. Conformations of 5/6, 4/6, and 3/6 were constructed (figures 6(a)–(c)), with the opened edges changed according to these conformations. The connection strands that could be used to hook the up and bottom edges were selected; next, these edges were opened and attached to the mica surface to a plane shape. The experimental protocol was the same as that used to develop the hexagonal origami structure. All strands were mixed (1:10 ratio) and annealed linearly at temperatures ranging from 95 °C to 4 °C. AFM images of the opened conformations (figures 6(d)–(i)) clearly showed the open and closed parts. The opened conformations were not robust, as they resembled broken strings in solution; however, the topological differences among the diverse formations could be distinguished. Moreover, as shown in figure 5, the end region of the linear origami demonstrated a concave-convex shape. We performed truncation of four double helices

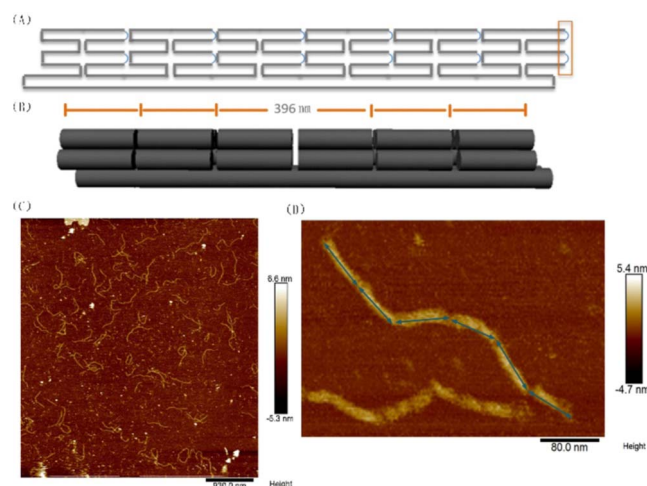


Figure 6. Linear origami structures. (a) Design scheme of the linear origami structures. The blue lines (highlighted in the yellow box) represent unpaired connection sequences. (b) Representation of the length of the linear origami structures. (c) Atomic force microscopy images of the linear origami structures. Scan size: 4.6 μm . (d) Detailed view of the six edges, scale size: 0.4 μm .

as shown in the left panel of figure 5(A). Next, the corresponding four double helices (as shown in the yellow box) protruded from the right end. As complementary ends are stacked together by base forces, the concave and convex ends can demonstrate the achievement of a topological connection. The DNA origami topological connection force was stronger than that of base pairing. As the base stacking force (hydrophobicity force) was used, these linear origins could be expected to be steadily linked.

A hierarchical annealing protocol was implemented to bind the linear origami structures. First, the annealing protocol was the same as that used to assemble a single origami structure. Second, the purified origami structures were linearly reannealed at temperatures ranging from 50 °C to 4 °C for 10 h. The initial incubation temperature was 50 °C and was considered as a mild temperature suitable for molecular thermodynamics. Molecular thermal motion is extremely active at this temperature, providing a high probability for base stacking (topological connection). However, this temperature is not adequately high to disrupt the structures. Representative AFM images (figure 7) showed that the connected assemblies were mostly dipolymers. A typical structure was selected for further analysis, and one assembly was scanned (figure 7(b)). Large assemblies were rare possibly because of the low connection efficiency; thus, a larger assembly could not easily form because the connection rate was markedly reduced in size [11, 15, 20].

In summary, the structure of a flexible hexagonal origami, with biotin-streptavidin-labeled edges, is described. The distance of each label in this origami was determined by the length of the edge. Additionally, we designed linear origami in two different batches; the short structure was assembled based on the first five edges of the hexagonal origami as a comparison sample. The longer structure was redesigned and programmed to resemble a rod-like shape in a different batch. Next, we performed experiments to open

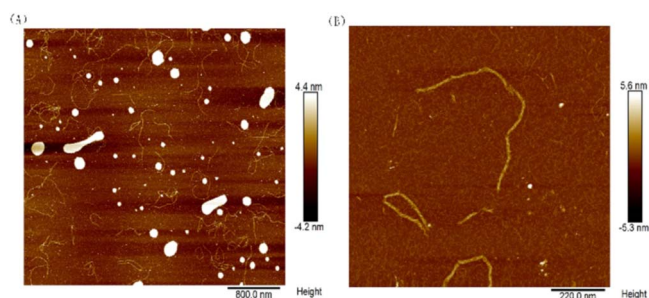


Figure 7. Atomic force microscopy imaging of the topological connection. Scan size: (a) 4.0 and (b) 1.2 μm .

specific edges of the linear origami to achieve three different conformations. These open edges were similar to ribbons, whereas the closed edges were similar to tubes. Additionally, the linear origami structure was designed with a concave-convex shape to enable the establishment of topological connections.

Collectively, these results demonstrate that this hexagonal origami is flexible, with the bottom helices functioning as hinges that hold the six edges together. Hence, this flexible origami composed of proteins can be used to match viral transient conformations. Future studies are warranted to explore the potential use of this origami bound to antigens to explore the spatial pattern of specific viruses.

Acknowledgments

This work was supported by the National Key R&D Program of China (grant number: 2019YFA0706401) and National Natural Science Foundation of China (grant numbers: 61772376, 61872166, 61632002, and 62072129). China Postdoctoral Science Foundation 2020M680237. The funding agencies played no role in the collection, analysis, and interpretation of data, in the writing of the report, or in the decision to submit the article for publication.

Data availability statement

All data that support the findings of this study are included within the article (and any supplementary files).

Conflict of interests

There are no conflicts to declare.

Authors' contributions

CZC and TTL performed the experiments. XLS and XL designed the experiments. CZC and MYM analyzed the data. CZC and XLS wrote the manuscript. All authors have read and approved the publication of the manuscript.

ORCID iDs

Congzhou Chen  <https://orcid.org/0000-0001-8425-3416>

References

- [1] Seeman N C 2003 *Nature* **421** 427–31
- [2] Adleman L M 1998 *Sci. Am.* **279** 54–61
- [3] Paun G, Rozenberg G and Salomaa A 2000 *DNA Computing: New Computing Paradigms* 15 (Springer Science & Business Media) 536
- [4] Zhang Q, Jiang Q, Li N, Dai L, Liu Q, Song L, Wang J, Li Y, Tian J and Ding B 2014 *ACS Nano* **8** 6633–43
- [5] Li Q, Zhao D, Shao X, Lin S, Xie X, Liu M, Ma W, Shi S and Lin Y 2017 *ACS Appl. Mater. Interfaces* **9** 36695–701
- [6] Yan H, Park S H, Finkelstein G, Reif J H and LaBean T H 2003 *Science* **301** 1882–4
- [7] Liu Q, Wang L, Frutos A G, Condon A E, Corn R M and Smith L M 2000 *Nature* **403** 175–9
- [8] Xu J, Qiang X, Zhang K, Zhang C and Yang J 2018 *Engineering* **4** 61–77
- [9] Liu C, Liu Y, Zhu E, Zhang Q, Wei X and Wang B 2020 *Nucleic Acids Res.* **48** 10691–701
- [10] Xiaolong S, Wei L, Zhiyu W, Linqiang P, Guangzhao C, Jin X and Labeau T H 2014 *Nanotechnology* **25** 075602
- [11] Tikhomirov G, Petersen P and Qian L 2017 *Nature* **552** 67
- [12] Brook I 1991 *J. Pediatric Surg.* **26** 207–9
- [13] Funke J J and Dietz H 2016 *Nat. Nanotechnol.* **11** 47–52
- [14] Rothmund P W 2006 *Nature* **440** 297
- [15] Chen C, Xu J and Shi X 2020 *Nanoscale* **12** 15066–71
- [16] Yan H, Yin P, Park S H, Li H, Feng L, Guan X, Liu D, Reif J H and LaBean T H 2004 *AIP Conf. Proc.* **725** 43
- [17] Tikhomirov G, Petersen P and Qian L 2017 *Nat. Nanotechnol.* **12** 251–9
- [18] Praetorius F, Kick B, Behler K L, Honemann M N, Weuster-Botz D and Dietz H 2017 *Nature* **552** 84
- [19] Han D, Pal S, Nangreave J, Deng Z, Liu Y and Yan H 2011 *Science* **332** 342–6
- [20] Iinuma R, Ke Y, Jungmann R, Schlichthaerle T, Woehrstein J B and Yin P 2014 *Science* **344** 65–9
- [21] Ong L L et al 2017 *Nature* **552** 72–7
- [22] Xiong Q, Xie C, Zhang Z, Liu L, Powell J T, Shen Q and Lin C 2020 *Angew. Chem. Int. Ed.* **59** 3956–60
- [23] Liber M, Tomov T E, Tsukanov R, Berger Y and Nir E 2015 *Small* **11** 568–75
- [24] Nickels P C, Wunsch B, Holzmeister P, Bae W, Kneer L M, Grohmann D, Tinnefeld P and Liedl T 2016 *Science* **354** 305–7
- [25] Wickham S F, Bath J, Katsuda Y, Endo M, Hidaka K, Sugiyama H and Turberfield A J 2012 *Nat. Nanotechnol.* **7** 169–73
- [26] Ketterer P, Willner E M and Dietz H 2016 *Sci. Adv.* **2** e1501209–1501209
- [27] Rinker S, Ke Y, Liu Y, Chhabra R and Yan H 2008 *Nat. Nanotechnol.* **3** 418–22
- [28] Shaw A, Lundin V, Petrova E, Fordos F, Benson E, Al-Amin A, Herland A, Blokzijl A, Hogberg B and Teixeira A I 2014 *Nat. Methods* **11** 841–6
- [29] Shaw A, Hoffecker I T, Smyrlaki I, Rosa J, Grevys A, Bratlie D, Sandlie I, Michaelsen T E, Andersen J T and Hogberg B 2019 *Nat. Nanotechnol.* **14** 184–90
- [30] Veneziano R et al 2020 *Nat. Nanotechnol.* **15** 716–23
- [31] Kwon P S et al 2020 *Nat. Chem.* **12** 26–35
- [32] Zhang P et al 2020 *Nat. Commun.* **11** 3114
- [33] Schellman J A and Harvey S C 1995 *Biophys. Chem.* **55** 95–114